HHS Public Access

Author manuscript

Biofabrication. Author manuscript; available in PMC 2024 May 01.

Published in final edited form as:

Biofabrication. ; 12(1): 015014. doi:10.1088/1758-5090/ab4c0a.

Glial cells influence cardiac permittivity as evidenced through *in vitro* and *in silico* models

Jonathan R Soucy[1], **Jody Askaryan**[1], **David Diaz**[1], **Abigail N Koppes**[1,2], **Nasim Annabi**[3,4,5], **Ryan A Koppes**[1,6]

[1]Department of Chemical Engineering, Northeastern University, Boston, MA 02115, United States of America

[2]Department of Biology, Northeastern University, Boston, MA 02115, United States of America

[3]Department of Chemical and Biomolecular Engineering, University of California-Los Angeles, Los Angeles, CA 90095, United States of America

[4]Center for Minimally Invasive Therapeutics (C-MIT), University of California-Los Angeles, Los Angeles, CA 90095, United States of America

[5]Harvard-MIT Division of Health Sciences and Technology, Massachusetts Institute of Technology, Cambridge, MA 02139, United States of America

[6]Authors to whom any correspondence should be addressed.

Abstract

Excitation–contraction (EC) coupling in the heart has, until recently, been solely accredited to cardiomyocytes. The inherent complexities of the heart make it difficult to examine non-muscle contributions to contraction *in vivo,* and conventional *in vitro* models fail to capture multiple features and cellular heterogeneity of the myocardium. Here, we report on the development of a 3D cardiac *μ*Tissue to investigate changes in the cellular composition of native myocardium *in vitro*. Cells are encapsulated within micropatterned gelatin-based hydrogels formed via visible light photocrosslinking. This system enables spatial control of the microarchitecture, perturbation of the cellular composition, and functional measures of EC coupling via video microscopy and a custom algorithm to quantify beat frequency and degree of coordination. To demonstrate the robustness of these tools and evaluate the impact of altered cell population densities on cardiac *μ*Tissues, contractility and cell morphology were assessed with the inclusion of exogenous non-myelinating Schwann cells (SCs). Results demonstrate that the addition of exogenous SCs alter cardiomyocyte EC, profoundly inhibiting the response to electrical pacing.

n.annabi@northeastern.edu and r.koppes@northeastern.edu.

Contributions

JRS, NA, and RAK conceived the project. JRS synthesized and characterized materials, isolated neonatal rat cardiac cells, stained and imaged all samples, developed the MATLAB algorithm, and wrote the electrophysiology stimulation. JRS completed the *in vitro* cell studies with assistance from JA. DD isolated and purified and SCs from neonatal rats under the advisement of ANK. ANK provided intellectual input and advice. JRS and RAK analyzed the results, prepared the figures, and wrote the manuscript. All authors edited and provided feedback on the manuscript. RAK and NA supervised the work.

Supplementary material for this article is available online

Competing interests

The authors declare no competing interests.

Computational modeling of connexin-mediated coupling suggests that SCs impact cardiomyocyte resting potential and rectification following depolarization. Cardiac *μ*Tissues hold potential for examining the role of cellular heterogeneity in heart health, pathologies, and cellular therapies.

Keywords

tissue engineering; electrophysiology; cardiac; connexin; Schwann cells; excitation–contraction coupling

Ischemic heart disease remains a leading cause of death worldwide. While pharmacological interventions have improved life expectancy by mitigating key risk factors, therapeutic strategies for repairing the damaged myocardium have yet to become the clinical standard (Björnson et al 2016, Hashimoto et al 2018). Following infarct, delivery of autologous cells, including mesenchymal stem cells, cardiac stem cells, and endothelial progenitor cells, have yielded promising results at the benchtop, but inconsistent benefits in clinical trials (Malliaras and Marbán 2011, Hatzistergos and Vedenko 2017, Muller et al 2018, Tang et al 2018). To improve the efficacy of potential therapeutic strategies, new experimental models at the benchtop that enhance our fundamental understanding of the contribution of cardiac support cells are required.

In a healthy heart, cardiomyocytes (CMs) are the most abundant cells by volume, but only make up 25%–35% of the total myocardial cells (Pinto et al 2016, Zhou and Pu 2016, Pawlak et al 2018, Perbellini et al 2018, Skelly et al 2018). While the percentage of CMs in the heart is relatively accepted, there is a lack of consensus regarding the interstitial cell composition in the heart (Pinto et al 2016). Current perspectives suggest the presence of fibroblasts, endothelial cells, smooth muscle cells, pericytes, Schwann cells (SCs), macrophages, telocytes stem cells, conduction cells (pacemaker cells and Purkinje fibers), neurons, and atrial and ventricular CMs (Armour 1991, Gherghiceanu and Popescu 2012, Xin et al 2013, Nandi and Mishra 2015, Popescu et al 2015, Pinto et al 2016, Zhou and Pu 2016, Pawlak et al 2018, Perbellini et al 2018, Skelly et al 2018). Further, the role of electric-coupling of resident, non-myocyte cells such as fibroblasts (Sachse et al 2008), macrophages (Hulsmans et al 2017), telocytes (Sheng et al 2014), and stem cells (Mayourian et al 2016) has only recently been observed and modeled. Due to current experimental limitations, the investigation of these cell types and their interactions require a combination of *in vivo*, *in vitro, and in silico* examination. Not only is the composition of the heart diverse, but an accurate understanding of cellular interactions is critical to fully comprehend cardiac pathogenesis and aid the development of new therapeutic strategies (Pinto et al 2016, Iseoka et al 2018, Zamani et al 2018).

The development of robust and biomimetic *in vitro* models recapitulating key features of mesoscale architecture and heterogeneity of *in vivo* counterparts is essential for the study of fundamental biological processes. While traditional two-dimensional (2D) cell culture techniques have been used for decades and contributed greatly to the understanding of cardiomyocyte function, limitations such as atypical cell size and morphology, de-differentiation, and limited cell-cell contacts limit discovery (Natarajan et al 2011, Zuppinger 2016). Three-dimensional (3D) cell culture has helped to overcome some of

these limitations by providing more physiologically relevant microenvironments, imparting robust mechanical cues as well as intra- and extracellular adhesion complexes similar to native tissue (Li et al 2012, Ravi et al 2015, Zuppinger 2019). In typical 3D culture, cells are encapsulated within extracellular matrix (ECM) like materials to more closely mimic the *in vivo* tissue architecture (Tibbitt and Anseth 2009, Gonzalez-Diaz and Varghese 2016). However, current 3D culture models are often limited to simple geometries or require the use of complex and expensive micro-fabrication techniques or microfluidics to form more complex biomimetic 3D constructs. Cell printing has enabled the production of complex 3D structures *in vitro* (Mandrycky et al 2016), however, the shear forces that cell experience during processing have greatly precluded the use of sensitive cell types like CMs (Mitcheson et al 1998, Kacarevic et al 2018).

Photocrosslinkable hydrogels facilitate an alternative to 3D printing by patterning complex shapes and structures to recapitulate *in vivo* architecture of tissues including the heart (DeForest et al 2009, Yue et al 2015). However, the reliance on ultraviolet (UV) light in these systems may lead to reduced cell viability (Naseer et al 2017, Noshadi et al 2017a). Further, while photocrosslinkable materials are relatively inexpensive to synthesize, the specialized light sources required to polymerize the materials are prohibitively expensive for widespread use. More specifically, there are no *in vitro* models to investigate the impact of resident non-CM cells on cardiomyocyte function. Therefore, there remains a need to develop an alternative inexpensive approach for designing an *in vitro* 3D culture model that can be scaled to systematically examine the multicellular nature of the cardiovascular system.

To address these challenges, here, we describe the development of a biomimetic, 3D *in vitro* model (or cardiac μTissue) to examine the role of different cell types in the heart. Specially, primary cardiac cells were encapsulated at different ratios and variable geometries to assess the importance and function of SCs and the potential influence on local alignment. Previously, the role of SCs in the myocardium has remained difficult to assess *in vivo* as knock-out models are unviable due to abnormal cardiac development during embryogenesis (Lee et al 1995, Morris et al 1999, Barik et al 2016). Therefore, to better mimic the cardiac microenvironment and maintain CM phenotype *in vitro* (Saini et al 2015, Wanjare and Huang 2017), a photolithography technique was used to create cardiac μTissues of micropatterned gelatin methacrylate (GelMA) via an inexpensive visible light LED (405 nm) system. Cardiac μTissue functional output was evaluated on a cell-by-cell basis using a novel algorithm to measure beats per minute (BPM) as well as the degree of coordination (DoC). In addition, functional differences between visible and traditional UV light photocrosslinking systems for encapsulation were compared in patterned and unpatterned systems. As a proof of concept for the potential of these cardiac μTissues to study cardiovascular health and repair, the role of exogenous SC incorporation, an abundant cell type whose function in the heart remains unknown, was characterized (figure 1(A)). Lastly, a computational model of SC-CM coupling was developed to provide deeper insight into the underlying SC impact on CM electrophysiology.

1. Experimental procedures

1.1. GelMA synthesis and hydrogel fabrication

GelMA, derived from fish gelatin, was synthesized as previously reported (Nichol et al 2010). In brief, 8% (v/v) methacrylic anhydride (Sigma) was added to a 10% (w/v) fish gelatin (Sigma) solution in Dulbecco's Phosphate Buffered Saline (DPBS, Sigma). The product of this reaction was dialyzed (Spectra/Por 12–14kD, Fisher Scientific) using distilled water for 1 week, and then lyophilized for use on demand. GelMA hydrogel precursor solutions (7.5% (w/v)) were prepared in complete culture medium [Dulbecco's Modified Eagle Medium (DMEM) without phenol red (Sigma) supplemented with 10% fetal bovine serum (Sigma), 2 mM L-glutamine (Gibco), and 50 units ml^{-1} penicillin/streptomycin (Gibco)] with 0.5% (w/v) 2-hydroxy-1-(4-(hydroxyethoxy) phenyl)-2-methyl-1-propanone (Irgacure® 2959, CIBA Chemicals) or 0.5% lithium phenyl-2,4,6-trimethyl-benzoylphosphinate (LAP, Biobots) as photoinitiators. Hydrogel precursors were then photocrosslinked by exposure to UV light (365 nm) with an Omnicure S2000 (Excelitas Technologies) for Irgacure® containing precursor hydrogels or visible light (405 nm) with a 10 W LED (QUANS) for LAP containing precursor hydrogels (0.25 s of 10 mW cm^{-2} light exposure per μm of hydrogel thickness).

1.2. Mechanical characterization

The compressive modulus of each hydrogel formulation (5%, 10%, and 15% (w/v) polymer concentration for UV and visible light crosslinked hydrogels) was examined using an ElectroForce mechanical load frame (TA instruments) with a 1000 gr load cell. Hydrogel samples were prepared in custom polydimethylsiloxane (Sylgard) molds (cylinders of 6 mm diameter; 4 mm height). Hydrogels were loaded between two compression platens, and cyclic uniaxial compression tests were conducted at 0.5 Hz (10 cycles). Compression displacement and load for each cycle were recorded using WinTest7 software. The compressive modulus was calculated as the tangent slope of the linear region of the stress–strain curves between 0.1 and 0.25 stain level. Three independently prepared samples for each formulation were measured to quantify the compressive modulus.

1.3. Primary cardiac cell isolation

Primary CMs and adherent cardiac cells (aCCs) were isolated from two-day old (p2) Sprague-Dawley neonatal rat (Charles River) hearts, following a modified protocol by Noshadi et al (2017b) and approved by Northeastern's Institutional Animal Care and Use Committee (IACUC). In brief, the thorax was opened and the heart was removed. The major veins and atria were then removed so that only the left and right ventricles remained. The ventricles were cut into 3–4 pieces and stored in 0.05% (v/v) trypsin (Gibco) in Hank's balanced salt solution (HBSS, Gibco) at 4 °C with continuous shaking overnight. The following day, the ventricle pieces were removed from the trypsin and subject to sequential collagenase treatments (305 units Collagenase II (Gibco) in HBSS) at 37 °C to dissociate the connective tissue and collect cardiac cells. Cells were then filtered through a 70 μm cell strainer (Falcon) and pre-plated in a tissue culture flask (T-175, Corning) with complete culture medium to enrich the CM population by differential adhesion. After one hour in standard cell culture conditions (37 °C, 5% CO_2), any unattached cells were

considered to be CMs, while those attached cells were deemed aCCs. Each cell population was then counted and used for experimentation within one hour following completion of the pre-plating enrichment.

1.4. SCs isolation

Primary SCs were isolated from p2 Sprague-Dawley neonatal rat sciatic nerves using established protocols (Koppes et al 2014, Soucy et al 2018). Sciatic nerves were harvested and kept in complete culture medium on ice for a maximum of 4 h. Dissected nerves were minced into 1–2 mm pieces under sterile conditions and incubated in a 6-well plate using complete culture medium in standard conditions. Tissue were then transferred to a new dish after visual confirmation of fibroblast migration. Three to four days after SC migration, cells were cultured with complete medium supplemented with 10^{-5} M cytosine arabinoside (Sigma) for 72 h to remove remaining highly mitotic fibroblasts. Next, a complement-mediated cell lysis was used to eliminate remaining fibroblasts. Cells were detached with 0.25% (v/v) trypsin/EDTA (Corning) and pelleted at 200 g for 5 min. Fibroblasts were targeted by re-suspending in 1 mL anti-CD90/Thy 1.1 (diluted 1:500 v/v in DMEM, Cedar Lane Labs) and incubated under standard conditions for 30 min. Treated cells were pelleted, re-suspended in 1 mL rabbit complement, and incubated for 30 min with standard conditions to selectively lyse the fibroblasts. After incubation, cells were centrifuged, re-suspended in SC maintenance medium (complete medium supplemented with 6.6 mM forskolin (Sigma) and 10 μg ml^{-1} bovine pituitary extract (Corning)), and cultured in a flask for expansion. Lysis was repeated if fibroblast impurities remained. SC purity was assessed using anti S-100 (DAKO). Maintenance medium was changed every other day and SCs were passaged before 100% confluency until P10.

1.5. 3D cell encapsulation

Equal parts of enriched CMs and aCCs (1:1), or CMs, aCCs, and SCs (1:1:1), were mixed with the hydrogel precursor solution (7.5% GelMA (w/v) and 0.5% (w/ v) Irgacure® or LAP) at a density of 1.5×10^7 cells ml^{-1}. Approximately 10 μl cell-laden gel precursor solution was placed between a 180 μm tall spacer and a 3-(trimethoxysilyl) propyl methacrylate (ACROS Organics) coated glass slide, followed by 45 s (10 mW cm^{-2}) light exposure through a laser cut black cardstock paper photomask (500 μm lines) to form patterned cell-laden hydrogels. Samples were incubated for 10 d in standard culture conditions with medium replaced every other day. Cell viability within 3D cardiac μTissues was determined via a LIVE/DEAD® viability/cytotoxicity kit (Life Technologies) one day post encapsulation.

1.6. Cardiac beating quantification

Individual CM contractions within the 3D μTissues were quantified with a custom MATLAB (Mathworks) code to calculate BPM on a cell-by-cell basis using video microscopy. Cardiac cells were recorded at 30 frames per second with phase contrast on a Zeiss Axio Observer at 20x with an incubation chamber (37 °C and 5% CO_2). Raw video files were exported as AVIs (M-JPEG compression, 90% quality) and imported into MATLAB for analysis. Regions of interest (ROIs) were identified from the first frame of the video recording as objects between 75 and 1000 μm^2 in size (figure S1(A) is available online at

stacks.iop.org/BF/12/015014/mmedia). To quantify BPM, the sum differences in frame-to-frame pixel intensity were measured for each ROI. Inclusion criteria for a beating CM was: (1) peak amplitude was greater than one standard deviation above the mean, (2) negative spikes were less than two standard deviations below the mean, and (3) the frequency of spikes was below 6 Hz (figures S1(B), (C)). After passing these prerequisites, beating was recorded as the number of spikes found in inclusion criteria 1. However, for high frame rate movies (frames per second >10), both CM contraction and relaxation may result in recorded spikes (figure S1(D)). To record only a single beat per contraction, the mean inter-spike-interval was calculated for each cell and spikes occurring below this value were disregarded. The average BPM was then calculated as the mean number of contractions for all ROIs in field of view ($m > 20$) multiplied by 60 and divided by the video length from a minimum of three samples per condition ($n > 3$).

To validate of accuracy and precision of this algorithm for measuring CM beating, simultaneous video microscopy (Axio Examiner at 40x) and electrical potential via a multielectrode array (MEA, multichannel systems) recordings were acquired and compared. Timestamps for each contraction from the identified CMs were assigned a unique identification number to gather a quantification on the degree of coordinated contraction in the μTissue models. Specifically, timestamped contraction data was imported into a modified algorithm originally developed to investigate neuronal activity (Kreuz et al 2015), and values of one minus the SPIKE-distance, an estimator of the similarity between spike trains, were reported as a means to quantify degree of coordinated CM contractions.

1.7. External electrical pacing

Electrical pacing of CMs was assessed using a chamber designed to apply pulsatile electrical stimuli (Tandon et al 2009) (50% duty square waves) to patterned cell-laden hydrogels at increasing frequencies (0.5, 1, 2, and 3 Hz) and voltage (1, 3, and 5 V) for 30 s. Alternating electrical stimulation was applied via two carbon rod electrodes mounted in a glass petri dish 2 cm apart. Pulsatile electrical signals were applied using a function generator (Agilent) connected to each carbon electrode with platinum wires. Alternating current stimulation was implemented to minimize hydrolysis. The chamber was filled with complete medium and each cell-laden hydrogel μTissue was aligned along the axis of the applied electric field between the two electrodes. The battery of conditions was randomized across samples to negate influence of testing order, and a minimum of five samples were examined at all frequencies and voltages.

1.8. Immunocytochemistry

Cell-laden μTissues were fixed with 4% paraformaldehyde (30 min), permeabilized with 0.1% X-100 Triton (20 min), then blocked with 5% goat serum (>12 h) in DPBS. After overnight blocking, samples were incubated in 1:400 rabbit anti S-100 (DAKO, Z0311), 1:200 mouse anti sarcomeric α-actinin (Abcam, ab9465), mouse anti CD90, and/or 1:200 goat anti connexin-43 (Abcam, ab87645) in blocking solution overnight at 4 °C. Cell-laden hydrogels were then washed thrice with DPBS and anti-rabbit, anti-mouse, and anti-goat secondary antibodies (1:200 in goat serum) were added overnight at 4 °C. Samples were rinsed with DPBS and mounted on cover slides with ProLong® Gold Antifade with 4’,6-

diamidino-2-phenylindole (DAPI). Lastly, the constructs were imaged using an inverted fluorescence microscope (Zeiss Axio Observer Z1).

1.9. Computational model of SC-CM Coupling

SC electrophysiological properties were mathematically simulated by curve fitting published voltage clamp data to a Hodgkin–Huxley model using MATLAB. Specifically, type I potassium (Baker and Ritchie 1996), L-type calcium (Amédée et al 1991), and the sodium currents (Howe and Ritchie 1990) were incorporated into this model. The electrophysiology properties of a beating cardiomyocyte coupled to a SC was modeled as previously described (Sachse et al 2008). Model parameters are expanded upon in supplementary information.

1.10. Statistical analysis

All data was first determined to be normally distributed using the Lilliefors test in MATLAB. Normally distributed data was compared in MATLAB by using a student-t test for data sets containing only two experimental conditions (figure 6(D)), a one-way ANOVA for experiments with more than two conditions (figures 1(C), 2(E), 4C, and 6(A), (B)), and a multi-way ANOVA for comparisons across multiple days (figures 3 and 5(A), (B)). Non-normally distributed data was compared in MATLAB with the Kruskal–Wallis test (figure 5G). A minimum of three images from three independent samples were analyzed to quantify viability, aspect ratio, and total cell percentage. Error bars represent the mean ± standard deviation of measurements (**$p < 0.05$).

2. Results

2.1. Cardiac tissue models

3D cardiac cultures were developed to rapidly and inexpensively synthesize μTissues. GelMA hydrogels were crosslinked with either a UV or visible light photoinitiator system: Irgacure® using an Omnicure S2000 (365 nm) or LAP using a custom 405 nm LED system (figure S2(A)). The compressive modulus of the visible crosslinked hydrogels increased significantly from 1.16 ± 0.04 kPa for 5% (w/v) GelMA to 22.56 ± 1.91 kPa for 10% GelMA to 80.49 ± 2.75 kPa for 15% GelMA (figure S2(B)). Based on these data, a 7.5% (w/v) GelMA hydrogel was selected to best mimic the stiffness of the native cardiac tissue (mean 6.8 kPa) (Bhana et al 2010).

Primary cardiac cells were encapsulated in patterned (500 μm wide lines; 2 mm separation) GelMA hydrogels by controlling the areas of the precursor hydrogel that were exposed to light using laser cut black cardstock paper (figure 1(B)). 3D μTissues exhibited increased viability (93.44 ± 3.75) compared to constructs formed with UV light, irrespective of the photoinitiator (figures 1(C) and S3). This method was used to fabricate a range of 3D geometries conventionally only achievable using microfluidics or bioprinting (figure 1(D)). Further, by adjusting the height of spacers from 180 μm to 360 or 540 μm, we demonstrated the ability to form a range of μTissue thicknesses as well as assembling layers of different compositions (figure 1(E)). However, despite our ability to increase μTissue thickness, a nutrient diffusion limitation would exist for hydrogels >300 μm that may significantly decrease CM viability (Lovett et al 2009, Figueiredo et al 2018, Sawyer et al 2018).

2.2. Functional characterization of cardiac output

To overcome the challenges associated with recording electrical potentials in 3D cultures as well as mitigate the financial hurdle of electrophysiology equipment, video microscopy has been used to measure cardiac frequency (Annabi et al 2013, Huebsch et al 2015, Saini et al 2015). However, this method does not account for the DoC between CM contractions, an important indicator of myocardium maturity. To determine isolated versus conducted contraction in our 3D *μ*Tissues, we developed an automated MATLAB algorithm to measure both CM BPM and DoC. Individual cells were identified within 3D *μ*Tissues (figure 2(A)) and classified as beating or a non-beating cardiac cells based upon inclusion criteria (i.e. signal-to-noise ratio, peak-to-peak frequency; figure 2(B)). The summation was used to calculate the global BPM for each experimental condition.

The DoC was quantified by assigning each beating CM with a unique cell ID# and plotting the time-stamp of each contraction (figure 2(C)). To quantify DoC, these plots were analyzed with a SPIKE algorithm developed for assessing synchrony in neuron populations (Kreuz et al 2015). As shown in figure 2(D), quantified cell beating using our developed algorithm has a one-to-one correlation with recordings processed using a MEA, demonstrating the robustness of our image analysis tool and that we are detecting CM depolarization (supplemental video 1). As further validation, *μ*Tissues were treated with isoproterenol, a beta-adrenergic agonist to demonstrate the utility of this algorithm to detect a changes in physiological responses (Maoz et al 2017). A temporal increase in beating frequency (~50%) and decrease in DoC (~10%) was detectable with this video quantification tool (figure 2(E)).

2.3. Impact of patterning and photoinitiator on 3D *μ*tissues

Spontaneous beating was recorded over a period of 9 d for cardiac *μ*Tissue constructs formed across all hydrogel samples. Similar to previous findings (Saini et al 2015), no beating was observed when only enriched populations of CMs were encapsulated within the 3D *μ*Tissues (data not shown). *μ*Tissues crosslinked with visible light (LAP), on average, exhibited on average a 25% increase in rates of beating for all measured time points compared to Irgacure® controls (figures 3(A)–(C)). There were no differences in the DoC were apparent when comparing crosslinking systems irrespective of patterning (figures 3(B), (C)). However, regardless of the crosslinking system implored, the inclusion of aCCs within patterned hydrogels led to spontaneous beating on day 3 post encapsulation versus day 4 post encapsulation for unpatterned samples (figures 3(A) and (D)). Lastly, despite the relatively low CM density, patterned 3D *μ*Tissues exhibited a statistically significant ($p < 0.0001$) increase in DoC compared to unpatterned hydrogels throughout the entire study (figures 3(E)–(F)).

2.4. SC incorporation in the 3D *μ*Tissues

To validate the use of cardiac *μ*Tissues for further understanding the role of non-myocyte support cells in the heart, CM functional outputs and morphological differences were assessed with the inclusion of exogenous SCs. Enriched CM and aCC populations were characterized via immunocytochemistry to quantify the endogenous cell composition as a baseline of isolation heterogeneity. As expected, an increased ratio of CMs, identified by

sarcomeric α-actinin, were present in the enriched CM suspension (figures 4(A)– (C)). The remaining non-adherent (enriched CM suspension) and adherent (aCCs) cells were identified by staining for fibroblasts ($CD90^+$), smooth muscle cells (α-smooth muscle $actin^+$), and SCs ($S100^+$). While, immunostaining demonstrated that both the enriched CM and aCC cultures contained heterogeneous cell populations, this analysis only provides a glimpse of all the cells found in the heart (Gherghiceanu and Popescu 2012, Nandi and Mishra 2015, Popescu et al 2015, Pinto et al 2016, Zhou and Pu 2016). However, by the reincorporation of all cell collected from the cardiac dissociation, the cardiac *μ*Tissues better recapitulate the cellular composition of an intact myocardium. The proportion of viable $S100^+$ cells isolated from the heart was 19.61% ± 4.08%, which is approximately double of the SC composition previously reported for the human atria (Popescu et al 2015). This higher than expected value, in part, may be due to false positives, specifically S100 expression in macrophages (Hulsmans et al 2017).

Injected SCs have demonstrated therapeutic effects on cardiac function following infarction in rodent models (Zhang et al 2010, Wang et al 2012). Here, SCs from the sciatic nerve were used to ensure a high concentration and avoid a potential loss of phenotype that has previously been reported for cardiac support cells during expansion (Zuppinger 2016). Inclusion of SCs led to a significant 2-fold increase ($p < 0.0001$) in the BPM of CMs as compared to controls at all measured time points (figures 5A, S4, supplemental video 2–3). Additionally, the inclusion of SCs decreased the DoC from 85.10% ± 0.98% to 76.76% ± 0.99% (figure 5(B)). These trends were also observed for cardiac cells with/without SCs when cultured on a 2D scaffold (figure S5). There were no observable morphological differences of CMs within the *μ*Tissues after the incorporation of SCs (figures 5(C), (D)), yet in 2D cultures, CMs co-cultured with SCs possessed an aspect ratio of 4.1 ± 1.8 compared to 1.6 ± 0.5 for controls without SCs (figures 5(E)–(G)).

2.5. Electrical pacing of 3D *μ*tissues

Electrical stimulation (ES) to pace the 3D *μ*Tissues provided better understand how SCs may influence contraction of the myocardium. ES was applied on day 5 post encapsulation via carbon rod electrodes as previously reported (Tandon et al 2009). BPM were measured for different frequencies and voltages of applied ES. Prior to ES, encapsulated cardiac cells had an average BPM of 45.27 ± 2.16. Ramping from 1 V to 3 V to 5 V led to an increased response that trended toward the applied frequency for 2 (117.19 ± 8.85) and 3 Hz (153.11 ± 6.95) at 5 V (figure 6(A)). The cardiac *μ*Tissues were unable to be paced at 0.5 or 1 Hz for any of the tested voltages. As the rate of spontaneous beating was close to the 1 Hz pacing, the effects of electrical stimulation in this range were indeterminable. The incorporation of SCs into these constructs (average BPM of 60.50 ± 9.51) completely prevented electrical pacing at any of the tested frequencies and voltages (figure 6(B)). Immunocytochemistry of the co-culture suggests that SCs ability to insulate CMs may in part be due to the formation of connexin junctions between SCs and CMs (figure 6(C)). Lastly, with the addition of a connexin blocker, heptanol, a small percentage of CMs exhibited increased beat rates when electrically stimulated (figure 6(D)), which were visually identified following slight increases in averaged beat rate with heptanol treatment (data not shown).

2.6. Modeling of CM-SC coupling

As evidence by visual analysis of 3D μTissues contractility, SCs influenced the electrophysiological properties of CMs *in vitro*. To further explore this interaction, we modeled CM-SC coupling *in silico* (figure 6(E)). We first developed a simple SC model by fitting published SC voltage clamp data for a type I potassium channel (Baker and Ritchie 1996), a L-type calcium channel (Amédée et al 1991), and a sodium channel (Howe and Ritchie 1990). Equations for maximum current, channel conductance, activation and inactivate coefficients, and time constants versus membrane potential were used to simulate voltage clamp experiments for each SC channel (figures S6–8). Coupling the simulated SC to a CM model *in silico* (Sachse et al 2008) suggested that SCs increase the CM resting potential and accelerates repolarization (figures 6(F)– (H)). *In vivo*, a decreased action potential duration for 90% repolarization (APD90) increases the frequency at which a CM can be depolarized (Hulsmans et al 2017), thereby increasing the maximum beating frequency. However, contrary to our results from electrical pacing, a higher resting potential did not reduce the stimulation threshold necessary to facilitate depolarization.

3. Discussion

Our developed biomimetic *in vitro* 3D μTissues hold potential to measure functional outputs as cardiac cellular composition is manipulated. This system approaches the resolution of cell printing without subjecting sensitive primary CMs to the temperatures and shear stresses often associated with bioprinting conditions (Blaeser et al 2016). GelMA allows tunability to mimic native mechanics, possesses protein composition to native myocardium ECM as well as a high availability of cell binding domains, and can be processed into 3D geometries (Yue et al 2015). But, traditional GelMA crosslinking requires high intensity UV and cytotoxic photoinitiators (Yue et al 2015) motivating the development of visible light crosslinking systems (Fairbanks et al 2009, Yue et al 2015, Annabi et al 2017, Noshadi et al 2017a).

EosinY/Triethanolamine is a type II photoinitiator that supports cell viability for encapsulated 3T3 fibroblasts (Noshadi et al 2017a), but poor viability for primary CMs (Noshadi et al 2017b) in crosslinked GelMA hydrogels. Type II photoinitiators also require longer photocrosslinking exposure times to achieve the same mechanical properties as type I photoinitiators (Fairbanks et al 2009), increasing free radicals that can impact viability (Maxwell and Lip 1997). However, in addition to the photocytotoxicity, Irgacure®, the most common type I photoinitiator used for crosslinking GelMA, is by itself cytotoxic (Fairbanks et al 2009). Therefore, we investigated the use of LAP, a commercially available visible light type I photoinitiation, for the development of our cardiac μTissues. GelMA hydrogels formed with either photoinitiator (LAP and Irgacure®) exhibited similar mechanical properties (figure S2(B)), within the ranges (~1–80 kPa) previously reported (Yue et al 2015). Primary cardiac cells encapsulated in GelMA hydrogels using LAP and visible light possessed higher cell viability than those formed by using UV light and/or Irgacure® (figure 1(C)), as reported previously in other cells (Fairbanks et al 2009).

Correlating in-the-dish measures of contractility to cardiac output and health is paramount for the long-term utility of *in vitro* cardiac models. BPM, DoC, and conduction velocity have been exclusively measured electrically (Natarajan et al 2011). However, methods for

intra and extracellular recordings require expensive equipment, specialized expertise, and use of these techniques with 3D *μ*Tissues provides additional technical challenges, such as reduced signal-to-noise ratios, low-throughput, and cell damage during the penetration of glass electrodes into the 3D *μ*Tissues (Tonomura et al 2010). Attempts to overcome these limitations have yielded some success by measuring contractions via video microscopy (Annabi et al 2013, Huebsch et al 2015, Saini et al 2015) or cantilevers (Boudou et al 2012, Morimoto et al 2013, Uzel et al 2016). In each of these cases, beating frequency is measured by counting the global changes in intensity, size, and/or force measurements over a set duration. These techniques fail to directly measure variability across individual beating cells, thus quantification of coordination and conduction velocity remain out of reach. Here, we developed a custom processing technique that allows for cardiac function to be assessed on a per cell basis that renders comparable results to traditional electrophysiology (figure 2). Further, due to our non-destructive imaging of cardiac beating, this approach may be used in combination with the previously mentioned techniques to correlate macroscopic function to intracellular interactions in both 2D and 3D culture systems. Our algorithm is capable of calculating conduction velocity, but accurate measures rely on frame rates faster than 200 frames per second to determine differences between cells, speeds which lies beyond the capabilities of most camera systems.

Towards investigating the effects of cardiac architecture, the role of patterning was assessed as an approach to improve function, specifically DoC. Maintaining coordinated beating in the heart is required *in vivo* to pump blood throughout the body, thus DoC is a critical metric to quantify for the establishment of cardiac *μ*Tissues. Previous studies have suggested local CM alignment is required to support synchronous beating and can be improved with micropatterned features having widths less than 100 *μ*m (Salick et al 2014, Saini et al 2015). Here, to study the sole impact of mesoscale architecture on DoC, *μ*Tissues were developed with widths of 500 *μ*m. As expected, there was no improved local, cellular alignment within patterned cardiac *μ*Tissues, but alignment of the cell-laden substrate resulted in an increase in DoC. Therefore, despite not exhibiting an alignment of CM along a single axis, patterned cardiac *μ*Tissues possess a higher degree of functionality towards recapitulating the native myocardium.

To understand how SCs might affect cardiomyocyte phenotype, we incorporated both primary SC and CM into *μ*Tissues. SCs are non-neural support cells that play an essential role in neuron signaling and regeneration (Armati and Mathey 2013). SCs have been evaluated at the bench as a cell therapy for cardiac failure (Zhang et al 2010, Wang et al 2012) and make up a substantial composition of the heart (Gherghiceanu and Popescu 2012, Popescu et al 2015). Often cells isolated from the heart are characterized as either CMs or cardiac FBs (Annabi et al 2013, Saini et al 2015, Annabi et al 2016, Shin et al 2016, Noshadi et al 2017a, 2017b), but in fact these populations are heterogeneous and contain fewer than 20% FBs. For this reason, we established a new nomenclature for this cell isolation protocol in which suspension cells are referred to as enriched CMs and the adherent cells are referred to as aCCs. Further, the presence of these aCCs is critical for developing functional engineered cardiac tissues from stem cells (Iseoka et al 2018).

CMs co-cultured with SCs in standard 2D conditions exhibited an increased aspect ratio (between 5 and 9.5; figures 5(A)–(C)), typical of a more mature CM phenotype (Denning et al 2016). Qualitatively, CMs cultured with SCs present with more clearly defined z-disks, evidenced by localization of α-actinin, elongation of nuclei, and a possible an increase in bi-nucleation (figure S9): indicators of CM differentiation and maturation (Scuderi and Butcher 2017, Zebrowski et al 2017). In response to peripheral nerve damage, non-myelinating SCs provide topographical cues that influence the rate and direction of neurite outgrowth (Hoffman-Kim et al 2010), with monolayers of SCs exhibiting beneficial local alignment that impacts sensory neuron growth *in vitro* (Seggio et al 2010). CMs may exhibit a higher aspect ratio via similar structural cues. Peculiar to this observation of increased CM differentiation, the presence of exogenous SCs increased the average BPM as well as a decrease the DoC in cardiac *μ*Tissues (figures 5(F)–(G)), similar to higher BPM observed during development (Lindsey et al 2014). However, immunofluorescent images of the CMs within the cardiac *μ*Tissues containing exogenous SCs did exhibit the higher aspect ratios observed in 2D cultures (figures 5(C)–(D)). Within a 3D scaffold, the mechanical microenvironment, specifically the increase in cell-ECM adhesions, may limit the influence of SC structure on CM morphology. Additionally, SC proliferation rate may be slowed (Edmondson et al 2014), limiting the density of SCs to promote local CM alignment.
In addition to providing guidance cues, SCs also overexpress matrix metalloproteinases (MMPs) following a nerve injury (Liu et al 2010, Parrinello et al 2010). Therefore, due to an abundance of MMP-sensitive degradation sequences in gelatin (Vandooren et al 2013), the inclusion of SCs may alter the mechanical properties of our *μ*Tissues over time, which may also influence cardiac phenotype and contraction (Bhana et al 2010). This reduction in mechanical stability was confirmed observationally by the increase degradation and delamination of the *μ*Tissues from the glass slides after 9 d (figure S10). Nevertheless, similar contractile trends were observed when cells were cultured on 2D scaffolds compared to those cultured in 3D, ruling out confounding effects of material degradation (figure S5).

Developing mammalian hearts beat at higher rates due a higher ratio of connective tissue to muscle or aCCs to CMs, immature T-tubule and sarcoplasmic reticulum, and a higher concentration of plasma calcium (Louch et al 2015). CM contraction is predominantly regulated by intracellular Ca^{2+} concentration cycling and a resultant membrane depolarization, that in mature CM constructs originates with an atrial pacemaker and progresses to surrounding cells with a high DoC. Non-myelinating SCs exhibit excitable properties including regulating Ca^{2+} in neuromuscular junctions (Reist and Smith 1992) and K^+ in the axonal microenvironment (Robert and Jirounek 1994). While SC presence in the heart has recently been highlighted, their role on plasma and cytosol ion dynamics in the myocardium remains unknown.

When external electrical stimulation was applied to 3D *μ*Tissues, SCs prevented the CMs within the *μ*Tissues from being externally paced. Similarly, Zhang et al reported that the injection of exogenous SCs into the heart reduced the occurrence of electrically induced arrhythmias (Zhang et al 2010). We hypothesize that SCs, which are known to express connexin proteins (Nicholson and Bruzzone 1997), form connexin junctions with some CMs (figure 6(C)), therefore increasing the resting potential and allowing for a more rapid depolarization and subsequent contraction and expansion. This mechanism of CMs forming

connexin junctions with other cells is demonstrated by a recent report in which cardiac macrophages are shown to increase the CM resting potential (Hulsmans et al 2017). While SCs maintain a higher resting membrane potential compared to CMs (−40 mV for SCs (Howe and Ritchie 1990, Baker and Ritchie 1996) versus −80 mV for CMs (Sachse et al 2008)), SCs also contain ion channels for Ca^{2+} and Na^{+} in addition to similar K^{+} channels to those in cardiac macrophages. Therefore, it is expected that in addition to an increased resting potential, the CM electrophysiological properties will be significantly altered by SC coupling.

Executing a CM-SC *in silico* model revealed that the initial depolarization of the SC membrane with CM depolarization led to an overcorrection to repolarize the SC membrane, which helped to quicken the CM repolarization. However, with increased coupling, the rate at which a CM is repolarized returned to its initial APD90, thereby suggesting an enhanced ability for CMs coupled with SCs to better regulate their membrane potential, while initial resting potential continues to increase. Lastly, when treated with a general connexin blocker, heptanol (Brokamp et al 2012), a small percentage of CMs responded to external, pulsatile electrical stimulus while non-blocked SC-CM cultures did not (figure 6(D)). These cells were visually identified and analyzed. While the proximity of these identified CMs to SCs was not known during live video recordings, this finding may support SCs ability to electrically couple to CMs via gap junctions, similar to that observed with fibroblasts (Sachse et al 2008) and macrophages (Hulsmans et al 2017). However, the mechanism which leads to increased beating and diminished coordination requires further investigation.

In conclusion, our 3D μTissues provide a cardiac cell-supporting microenvironment by better mimicking the function and cellular composition of the heart, which is critical for the development of cell and tissue engineering therapeutic strategies (Cimetta et al 2013). Furthermore, this platform can be exploited to investigate the multicellular composition of the heart via the inclusion of exogenous cell populations. Specially, utilizing this approach in combination with computational modeling, we demonstrated that SCs may play a critical role in CM maturation and as electrical insulators in the heart. This system may provide a means to model human physiology and pathology through the incorporation of stem cell derived cardiac cell populations. All together, these approaches in conjunction with computational models, quantitative cardiac outputs, and low capital expensive will hopefully lead to a more widespread use of microphysiological systems, which can be utilized to increase translation of novel therapies to the clinic. All algorithms for both analysis and modeling can downloaded from http://www.northeastern.edu/lnnr.

Supplementary Material

Refer to Web version on PubMed Central for supplementary material.

Acknowledgments

This work was supported by American Heart Association (AHA) Grant #19PRE34430181 (JR Soucy). RAK and NA acknowledge Northeastern University and the startup fund provided by the Department of Chemical Engineering, College of Engineering at Northeastern University. RAK further acknowledges the support from the National Institutes of Health (NIH, R21EB025395-01) and NA acknowledges the support from the AHA (16SDG31280010) and the NIH (R01-EB023052/O1A1).

References

Amédée T, Ellie E, Dupouy B and Vincent JD 1991 Voltage-dependent calcium and potassium channels in Schwann cells cultured from dorsal root ganglia of the mouse J. Physiol. 441 35–56 [PubMed: 1667796]

Annabi N, Rana D, Shirzaei Sani E, Portillo-Lara R, Gifford JL, Fares MM, Mithieux SM and Weiss AS 2017 Engineering a sprayable and elastic hydrogel adhesive with antimicrobial properties for wound healing Biomaterials 139 229–43 [PubMed: 28579065]

Annabi N et al. 2016 Highly elastic and conductive human-based protein hybrid hydrogels Adv. Mater. 28 40–9 [PubMed: 26551969]

Annabi N, Tsang K, Mithieux SM, Nikkhah M, Ameri A, Khademhosseini A and Weiss AS 2013 Highly elastic micropatterned hydrogel for engineering functional cardiac tissue Adv. Funct. Mater. 23 4950–9

Armati PJ and Mathey EK 2013 An update on Schwann cell biology–immunomodulation, neural regulation and other surprises J. Neurol. Sci. 333 68–72 [PubMed: 23422027]

Armour AJ 1991 Intrinsic cardiac neurons J. Cardiovascular Electrophysiol. 2 331–41

Baker MD and Ritchie JM 1996 Characteristics of type I and type II K+ channels in rabbit cultured Schwann cells J. Physiol. 49079–95 [PubMed: 8745280]

Barik A, Li L, Sathyamurthy A, Xiong CW and Mei L 2016 Schwann cells in neuromuscular junction formation and maintenance J. Neurosci. 36 9770–81 [PubMed: 27656017]

Bhana B, Iyer RK, Chen WL, Zhao R, Sider KL, Likhitpanichkul M, Simmons CA and Radisic M 2010 Influence of substrate stiffness on the phenotype of heart cells Biotechnol. Bioeng. 105 1148–60 [PubMed: 20014437]

Björnson E, Borén J and Mardinoglu A 2016 Personalized Cardiovascular disease prediction and treatment—a review of existing strategies and novel systems medicine tools Frontiers Physiol. 7 2

Blaeser A, Campos D, Puster U, Richtering W, Stevens MM and Fischer H 2016 Controlling shear stress in 3D bioprinting is a key factor to balance printing resolution and stem cell integrity Adv. Healthc. Mater. 5 326–33 [PubMed: 26626828]

Boudou T, Legant WR, Mu A, Borochin MA, Thavandiran N, Radisic M, Zandstra PW, Epstein JA, Margulies KB and Chen CS 2012 A microfabricated platform to measure and manipulate the mechanics of engineered cardiac microtissues Tissue Eng. A 18 910–9

Brokamp C, Todd J, Montemagno C and Wendell D 2012 Electrophysiology of single and aggregate Cx43 hemichannels PLoS One 7 e47775 [PubMed: 23112846]

Cimetta E, Godier-Furnémont A and Vunjak-Novakovic G 2013 Bioengineering heart tissue for in vitro testing Curr. Opin. Biotechnol. 24 926–32 [PubMed: 23932513]

DeForest CA, Polizzotti BD and Anseth KS 2009 Sequential click reactions for synthesizing and patterning three-dimensional cell microenvironments Nat. Mater. 8 659–64 [PubMed: 19543279]

Denning C et al. 2016 Cardiomyocytes from human pluripotent stem cells: From laboratory curiosity to industrial biomedical platform Biochim. Biophys. Acta 1863 1728–48 [PubMed: 26524115]

Edmondson R, Broglie JJ, Adcock AF and Yang L 2014 Three-dimensional cell culture systems and their applications in drug discovery and cell-based biosensors Assay Drug Dev. Technol. 12 207–18 [PubMed: 24831787]

Fairbanks BD, Schwartz MP, Bowman CN and Anseth KS 2009 Photoinitiated polymerization of PEG-diacrylate with lithium phenyl-2,4,6-trimethylbenzoylphosphinate: polymerization rate and cytocompatibility Biomaterials 30 6702–7 [PubMed: 19783300]

Figueiredo L, Pace R, D'Arros C, Rethore G, Guicheux J, Le Visage C and Weiss P 2018 Assessing glucose and oxygen diffusion in hydrogels for the rational design of 3D stem cell scaffolds in regenerative medicine J. Tissue Eng. Regen. Med. 12 1238–46 [PubMed: 29489057]

Gherghiceanu M and Popescu LM 2012 Cardiac telocytes—their junctions and functional implications Cell Tissue Res. 348 265–79 [PubMed: 22350946]

Gonzalez-Diaz EC and Varghese S 2016 Hydrogels as extracellular matrix analogs Gels 2 20 [PubMed: 30674152]

Hashimoto H, Olson EN and Bassel-Duby R 2018 Therapeutic approaches for cardiac regeneration and repair Nat. Rev. Cardiol. 15 585–600 [PubMed: 29872165]

Hatzistergos KE and Vedenko A 2017 Cardiac cell therapy 3.0: the beginning of the end or the end of the beginning? Circ. Res. 121 95–7 [PubMed: 28684618]

Hoffman-Kim D, Mitchel JA and Bellamkonda RV 2010 Topography, cell response, and nerve regeneration Annu. Rev. Biomed. Eng. 12 203–31 [PubMed: 20438370]

Howe JR and Ritchie JM 1990 Sodium currents in Schwann cells from myelinated and non-myelinated nerves of neonatal and adult rabbits J. Physiol. 425 169–210 [PubMed: 2170628]

Huebsch N et al. 2015 Automated video-based analysis of contractility and calcium flux in human-induced pluripotent stem-derived cardiomyocytes cultured over different spatial scales Tissue Eng. C 21 467–79

Hulsmans M et al. 2017 Macrophages facilitate electrical conduction in the heart Cell 169 510 [PubMed: 28431249]

Iseoka H et al. 2018 Pivotal role of non-cardiomyocytes in electromechanical and therapeutic potential of induced pluripotent stem cell-derived engineered cardiac tissue Tissue Eng. A 24 287–300

Kacarevic ZP, Rider PM, Alkildani S, Retnasingh S, Smeets R, Jung O, Ivanisevic Z and Barbeck M 2018 An introduction to 3D bioprinting: possibilities, challenges and future aspects Materials 11 2199 [PubMed: 30404222]

Koppes AN, Nordberg AL, Paolillo GM, Goodsell NM, Darwish HA, Zhang L and Thompson DM 2014 Electrical stimulation of Schwann cells promotes sustained increases in neurite outgrowth Tissue Eng. A 20 494–506

Kreuz T, Mulansky M and Bozanic N 2015 SPIKY: a graphical user interface for monitoring spike train synchrony J. Neurophysiol. 113 3432–45 [PubMed: 25744888]

Lee KF, Simon H, Chen H, Bates B, Hung MC and Hauser C 1995 Requirement for neuregulin receptor erbB2 in neural and cardiac development Nature 378 394–8 [PubMed: 7477377]

Li X, Valadez AV, Zuo P and Nie Z 2012 Microfluidic 3D cell culture: potential application for tissue-based bioassays Bioanalysis 4 1509–25 [PubMed: 22793034]

Lindsey SE, Butcher JT and Yalcin HC 2014 Mechanical regulation of cardiac development Frontiers Physiol. 5 318

Liu H, Kim Y, Chattopadhyay S, Shubayev I, Dolkas J and Shubayev VI 2010 Matrix metalloproteinase inhibition enhances the rate of nerve regeneration in vivo by promoting dedifferentiation and mitosis of supporting Schwann cells J. Neuropathol. Exp. Neurol. 69 386–95 [PubMed: 20448483]

Louch WE, Koivumäki JT and Tavi P 2015 Calcium signalling in developing cardiomyocytes: implications for model systems and disease J. Physiol. 593 1047–63 [PubMed: 25641733]

Lovett M, Lee K, Edwards A and Kaplan DL 2009 Vascularization strategies for tissue engineering Tissue Eng. B 15 353–70

Malliaras K and Marbán E 2011 Cardiac cell therapy: where we've been, where we are, and where we should be headed Br. Med. Bull. 98 161–85 [PubMed: 21652595]

Mandrycky C, Wang Z, Kim K and Kim D-H 2016 3D bioprinting for engineering complex tissues Biotechnol. Adv. 34 422–34 [PubMed: 26724184]

Maoz BM et al. 2017 Organs-on-Chips with combined multielectrode array and transepithelial electrical resistance measurement capabilities Lab Chip 17 2294–302 [PubMed: 28608907]

Maxwell SR and Lip GY 1997 Free radicals and antioxidants in cardiovascular disease Br. J. Clin. Pharmacol. 44 307–17 [PubMed: 9354304]

Mayourian J, Savizky RM, Sobie EA and Costa KD 2016 Modeling electrophysiological coupling and fusion between human mesenchymal stem cells and cardiomyocytes PLoS Comput. Biol. 12 e1005014

Mitcheson JS, Hancox JC and Levi AJ 1998 Cultured adult cardiac myocytes: Future applications, culture methods, morphological and electrophysiological properties Cardiovascular Res. 39 280–300

Morimoto Y, Kato-Negishi M, Onoe H and Takeuchi S 2013 Three-dimensional neuron-muscle constructs with neuromuscular junctions Biomaterials 34 9413–9 [PubMed: 24041425]

Morris JK, Lin W, Hauser C, Marchuk Y, Getman D and Lee KF 1999 Rescue of the cardiac defect in ErbB2 mutant mice reveals essential roles of ErbB2 in peripheral nervous system development Neuron 23 273–83 [PubMed: 10399934]

Muller P, Lemcke H and David R 2018 Stem cell therapy in heart diseases—cell types, mechanisms and improvement strategies Cell. Physiol. Biochem. 48 2607–55 [PubMed: 30121644]

Nandi SS and Mishra PK 2015 Harnessing fetal and adult genetic reprograming for therapy of heart disease J. Nat. Sci. 1 e71 [PubMed: 25879081]

Naseer SM et al. 2017 Surface acoustic waves induced micropatterning of cells in gelatin methacryloyl (GelMA) hydrogels Biofabrication 9 015020

Natarajan A, Stancescu M, Dhir V, Armstrong C, Sommerhage F, Hickman JJ and Molnar P 2011 Patterned cardiomyocytes on microelectrode arrays as a functional, high information content drug screening platform Biomaterials 32 4267–74 [PubMed: 21453966]

Nichol JW, Koshy ST, Bae H, Hwang CM, Yamanlar S and Khademhosseini A 2010 Cell-laden microengineered gelatin methacrylate hydrogels Biomaterials 31 5536–44 [PubMed: 20417964]

Nicholson SM and Bruzzone R 1997 Gap junctions: getting the message through Curr. Biol. 7 R340–44 [PubMed: 9197229]

Noshadi I et al. 2017a In vitro and in vivo analysis of visible light crosslinkable gelatin methacryloyl (GelMA) hydrogels. Biomaterials Science 5 2093–105 [PubMed: 28805830]

Noshadi I, Walker BW, Portillo-Lara R, Sani E, Gomes N, Aziziyan M and Annabi N 2017b Engineering biodegradable and biocompatible bio-ionic liquid conjugated hydrogels with tunable conductivity and mechanical properties Sci. Rep. 7 4345 [PubMed: 28659629]

Parrinello S, Napoli I, Ribeiro S, Wingfield Digby P, Fedorova M, Parkinson DB, Doddrell RD, Nakayama M, Adams RH and Lloyd AC 2010 EphB signaling directs peripheral nerve regeneration through Sox2-dependent Schwann cell sorting Cell 143 145–55 [PubMed: 20869108]

Pawlak M, Niescierowicz K and Winata CL 2018 Decoding the heart through next generation sequencing approaches Genes 9 289 [PubMed: 29880785]

Perbellini F, Watson SA, Bardi I and Terracciano CM 2018 Heterocellularity and cellular cross-talk in the cardiovascular system Frontiers Cardiovascular Med. 5 143

Pinto AR et al. 2016 Revisiting cardiac cellular composition Circ. Res. 118 400–9 [PubMed: 26635390]

Popescu LM, Curici A, Wang E, Zhang H, Hu S and Gherghiceanu M 2015 Telocytes and putative stem cells in ageing human heart J. Cell. Mol. Med. 19 31–45 [PubMed: 25545142]

Ravi M, Paramesh V, Kaviya SR, Anuradha E and Solomon FD 2015 3D cell culture systems: advantages and applicationsJ. Cell. Physiol. 230 16–26 [PubMed: 24912145]

Reist NE and Smith SJ 1992 Neurally evoked calcium transients in terminal Schwann cells at the neuromuscular junction Proc. Natl Acad. Sci. USA 89 7625–9 [PubMed: 1502174]

Robert A and Jirounek P 1994 Uptake of potassium by nonmyelinating Schwann cells induced by axonal activity J. Neurophysiol. 72 2570–9 [PubMed: 7897474]

Sachse FB, Moreno AP and Abildskov JA 2008 Electrophysiological modeling of fibroblasts and their interaction with myocytes Ann. Biomed. Eng. 36 41–56 [PubMed: 17999190]

Saini H, Navaei A, Van Putten A and Nikkhah M 2015 3D cardiac microtissues encapsulated with the co-culture of cardiomyocytes and cardiac fibroblasts Adv. Healthc. Mater. 4 1961–71 [PubMed: 26129820]

Salick MR, Napiwocki BN, Sha J, Knight GT, Chindhy SA, Kamp TJ, Ashton RS and Crone WC 2014 Micropattern width dependent sarcomere development in human ESC-derived cardiomyocytes Biomaterials 35 4454–64 [PubMed: 24582552]

Sawyer SW, Shridhar SV, Zhang K, Albrecht LD, Filip AB, Horton JA and Soman P 2018 Perfusion directed 3D mineral formation within cell-laden hydrogels Biofabrication 10 035013

Scuderi GJ and Butcher J 2017 Naturally engineered maturation of cardiomyocytes Frontiers Cell Dev. Biol. 5 50

Seggio AM, Narayanaswamy A, Roysam B and Thompson DM 2010 Self-aligned Schwann cell monolayers demonstrate an inherent ability to direct neurite outgrowth J. Neural Eng. 7 46001

Sheng J, Shim W, Lu J, Lim S, Ong B, Lim T, Liew R, Chua Y and Wong P 2014 Electrophysiology of human cardiac atrial and ventricular telocytes J. Cell. Mol. Med. 18 355–62 [PubMed: 24467431]

Shin S et al. 2016 Reduced graphene oxide-GelMA hybrid hydrogels as Scaffolds for cardiac tissue engineering Small 12 3677–89 [PubMed: 27254107]

Skelly DA, Squiers GT, McLellan MA, Bolisetty MT, Robson P, Rosenthal NA and Pinto AR 2018 Single-cell transcriptional profiling reveals cellular diversity and intercommunication in the mouse heart Cell Rep. 22 600–10 [PubMed: 29346760]

Soucy JR, Ehsan S, Roberto P, David D, Felipe D, Weiss AS, Koppes AN, Koppes RA and Nasim A 2018 Photocrosslinkable gelatin/tropoelastin hydrogel adhesives for peripheral nerve repair Tissue Eng. A 24 1393–405

Tandon N, Cannizzaro C, Chao P-HGH, Maidhof R, Marsano A, Au HT, Radisic M and Vunjak-Novakovic G 2009 Electrical stimulation systems for cardiac tissue engineering Nat. Protocols 4 155–73 [PubMed: 19180087]

Tang JN, Cores J, Huang K, Cui XL, Luo L, Zhang JY, Li TS, Qian L and Cheng K 2018 Concise review: is cardiac cell therapy dead? embarrassing trial outcomes and new directions for the future Stem Cells Transl. Med. 7 354–9 [PubMed: 29468830]

Tibbitt MW and Anseth KS 2009 Hydrogels as extracellular matrix mimics for 3D cell culture Biotechnol. Bioeng. 103 655–63 [PubMed: 19472329]

Tonomura W, Shimizu K and Konishi S 2010 Electrophysiological recordings using spatially arranged microelectrode probes embedded into 3D neuronal cultures Proc. MicroTAS2010

Uzel SG, Platt RJ, Subramanian V, Pearl TM, Rowlands CJ, Chan V, Boyer LA, So PT and Kamm RD 2016 Microfluidic device for the formation of optically excitable, three-dimensional, compartmentalized motor units Sci. Adv. 2 e1501429

Vandooren J, Van den Steen PE and Opdenakker G 2013 Biochemistry and molecular biology of gelatinase B or matrix metalloproteinase-9 (MMP-9): the next decade Crit. Rev. Biochem. Mol. Biol. 48 222–72 [PubMed: 23547785]

Wang Y et al. 2012 Transplantation of microencapsulated Schwann cells and mesenchymal stem cells augment angiogenesis and improve heart function Mol. Cell. Biochem. 366 139–47 [PubMed: 22488214]

Wanjare M and Huang NF 2017 Regulation of the microenvironment for cardiac tissue engineering Regen. Med. 12 187–201 [PubMed: 28244821]

Xin M, Olson EN and Bassel-Duby R 2013 Mending broken hearts: cardiac development as a basis for adult heart regeneration and repair Nat. Rev. Mol. Cell Biol. 14

Yue K, Trujillo-de Santiago G, Alvarez MM, Tamayol A, Annabi N and Khademhosseini A 2015 Synthesis, properties, and biomedical applications of gelatin methacryloyl (GelMA) hydrogels Biomaterials 73 254–71 [PubMed: 26414409]

Zamani M, Karaca E and Huang NF 2018 Multicellular interactions in 3D engineered myocardial tissue Frontiers Cardiovascular Med. 5 147

Zebrowski DC, Jensen CH, Becker R, Ferrazzi F, Baun C, Hvidsten S, Sheikh SP, Polizzotti BD, Andersen DC and Engel FB 2017 Cardiac injury of the newborn mammalian heart accelerates cardiomyocyte terminal differentiation Sci. Rep. 7 8362 [PubMed: 28827644]

Zhang H, Yuan X, Jin PF, Hou JF, Wang W, Wei YJ and Hu S 2010 Alteration of parasympathetic/sympathetic ratio in the infarcted myocardium after Schwann cell transplantation modified electrophysiological function of heart: a novel antiarrhythmic therapy Circulation 122 S193–200 [PubMed: 20837913]

Zhou P and Pu WT 2016 Recounting cardiac cellular composition Circ. Res. 118 368–70 [PubMed: 26846633]

Zuppinger C 2016 3D culture for cardiac cells Biochim. Biophys. Acta—Mol. Cell Res. 1863 1873–81

Zuppinger C 2019 3D cardiac cell culture: a critical review of current technologies and applications Frontiers Cardiovascular Med. 6 87

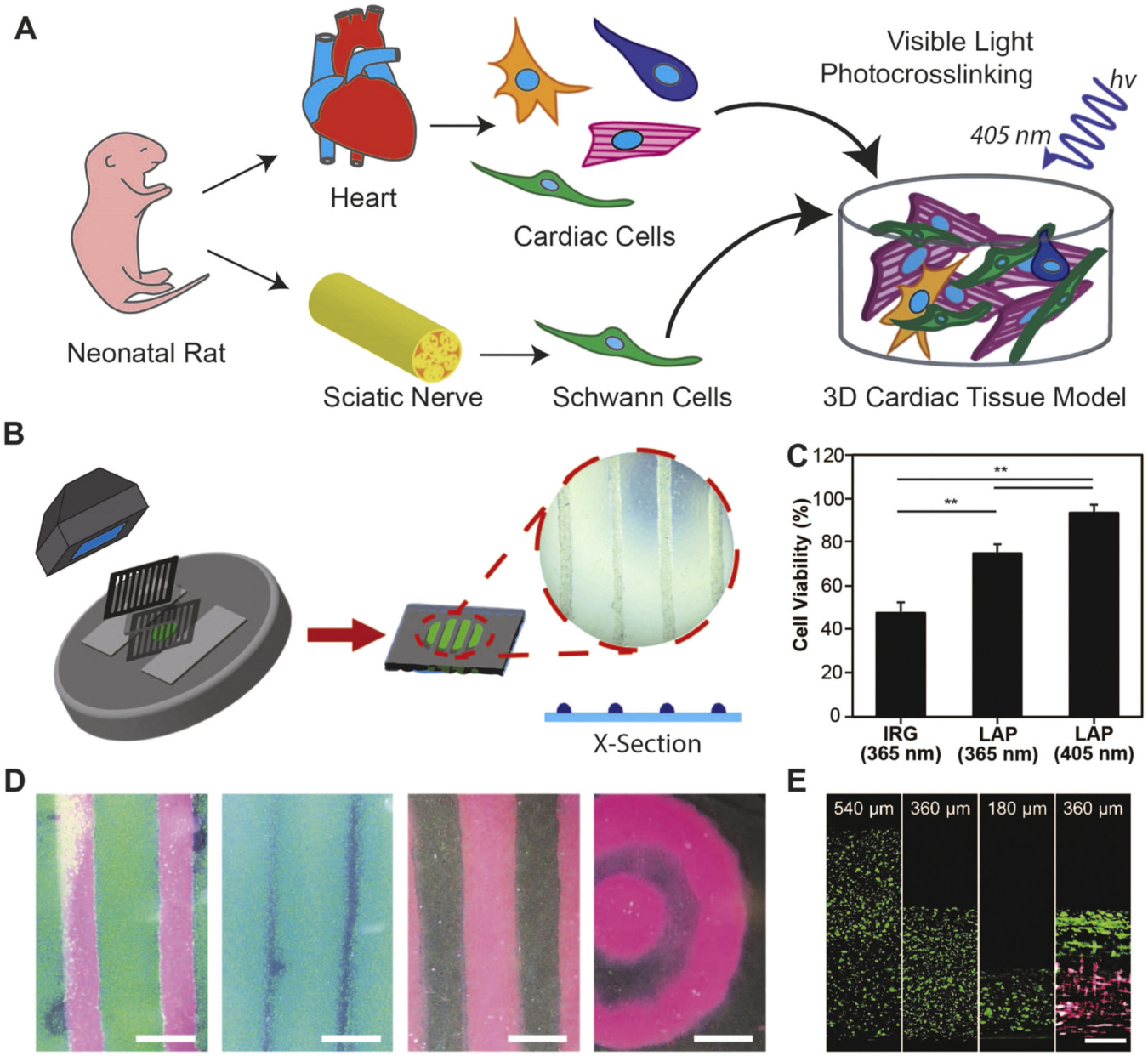

Figure 1.

Cardiac μTissue development. (A) Schematic representation of the in *vitro* co-culture system to investigate the heterogeneity of the myocardium. (B) Schematic of photopatterning hydrogels using visible light. (C) Quantification of live/dead images show >90% cardiac cell viability in GelMA crosslinked using LAP with visible light (**$p < 0.05$). IRG: Irgacure® 2959. LAP: phenyl-2,4,6-trimethylbenzoylphosphinate. (D) Representative images demonstrating an ability to photopattern a range of geometries (scale = 1000 μm) and (E) heights, including layers of different compositions, as shown by cross-sections of the 3D μTissues (scale = 100 μm).

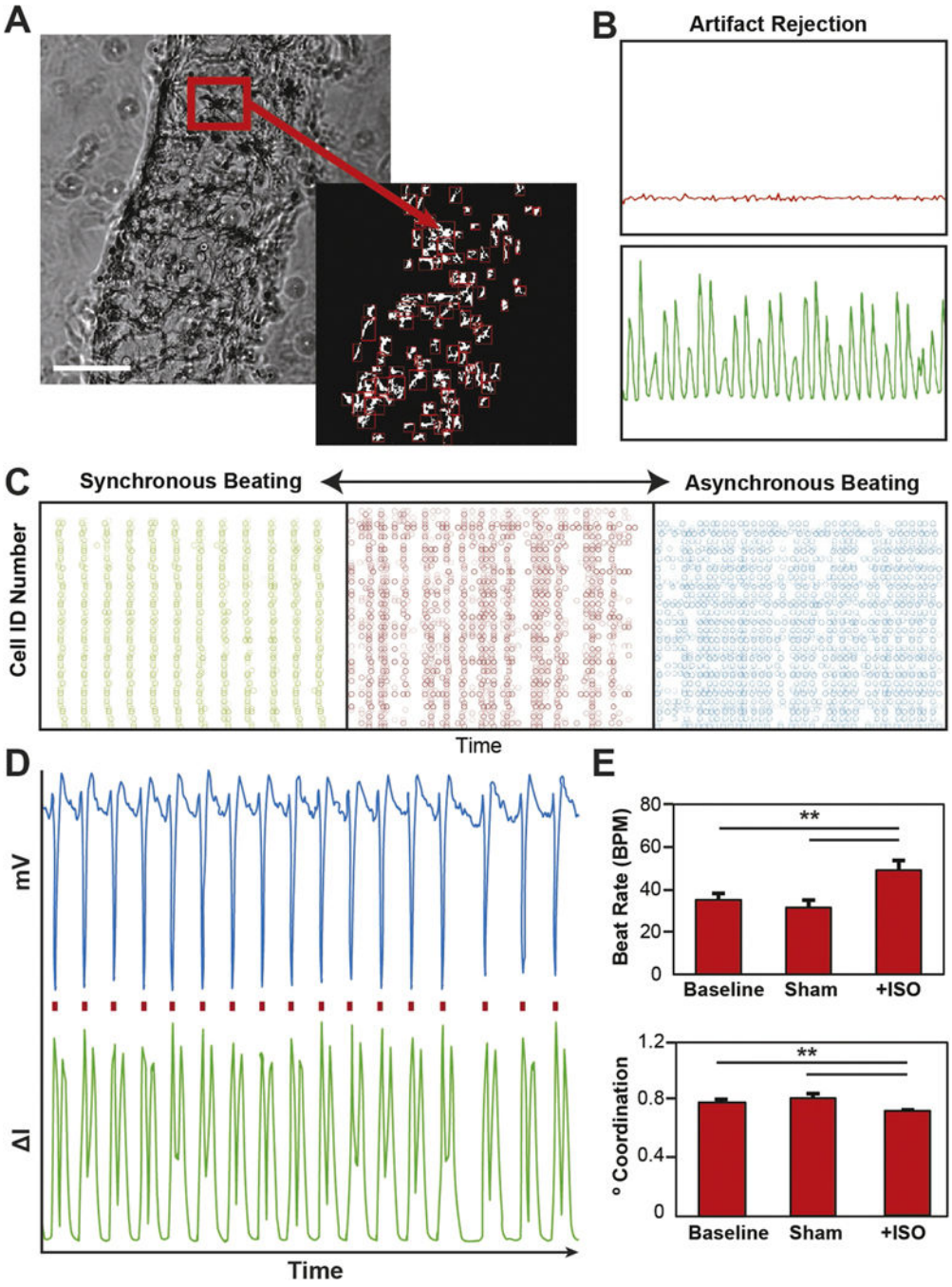

Figure 2.

Cardiac beating quantification via video microcopy. (A) Representative bright field image with automated identification of encapsulated cells (scale = 200 μm). (B) Representative plots showing the change pixel intensity over time for both a beating and non-beating cell. (C) Representative spike train analog used to quantify the degree of coordinated contractions (green = high level of synchrony, red = some semblance synchrony, blue = no apparent synchrony). (D) Validation of beating quantification shows a one-for-one correlation with electrophysiology recordings. (E) Isoproterenol treatment of encapsulated cardiac cells

shows an expected increase in beat rate and a decrease in synchrony measured via video microcopy (**$p < 0.05$).

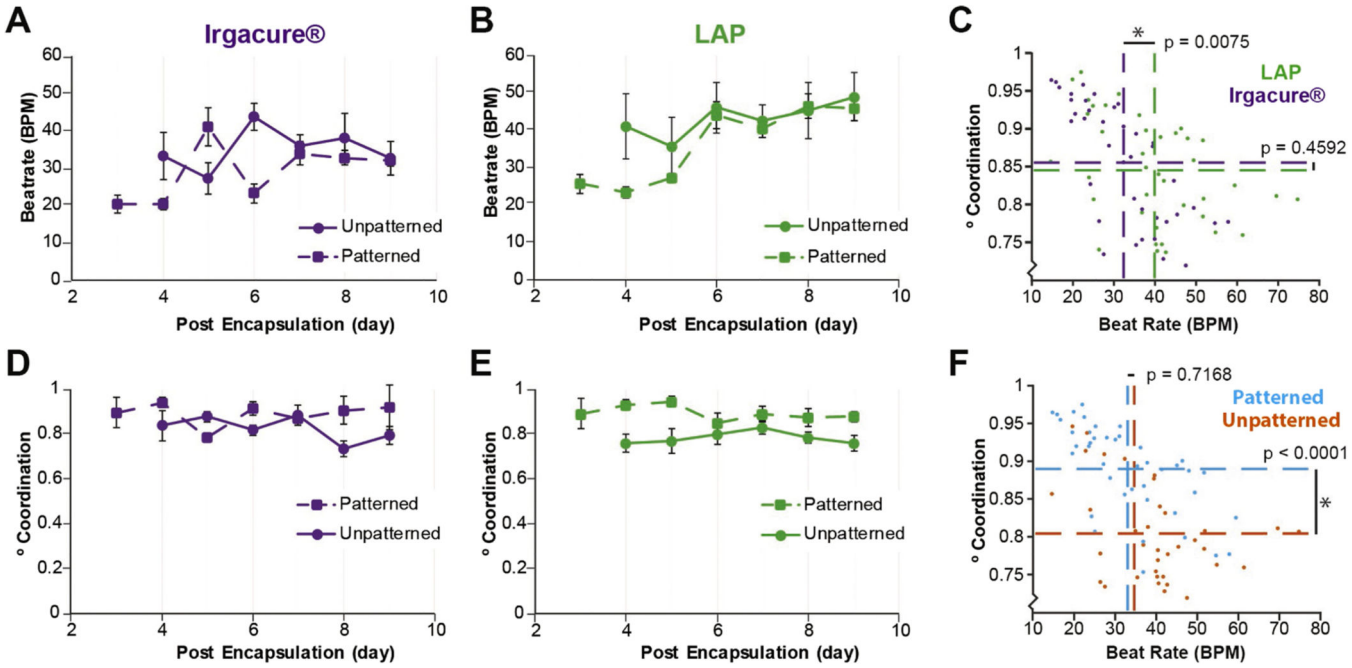

Figure 3.

Model development informed by cardiac output quantification. (A) Quantification of beat rate for cardiac cells encapsulated in unpatterned and patterned hydrogels over time using aUV(Irgacure® and 365 nm) or (B) a visible (LAP and 405 nm) or crosslinking system. (C) Multi-way ANOVA showing statistical differences between the visible and UV crosslinking systems for beat rate, but not coordination. (D) Quantification of DoC for cardiac cells encapsulated in patterned or unpatterned hydrogels formed using aUV (Irgacure® and 365 nm) or (E) visible light (LAP and 405 nm) crosslinking system. (F) Multi-way ANOVA showing statistical differences between patterned and unpatterned samples for beating coordination, but not beat rate.

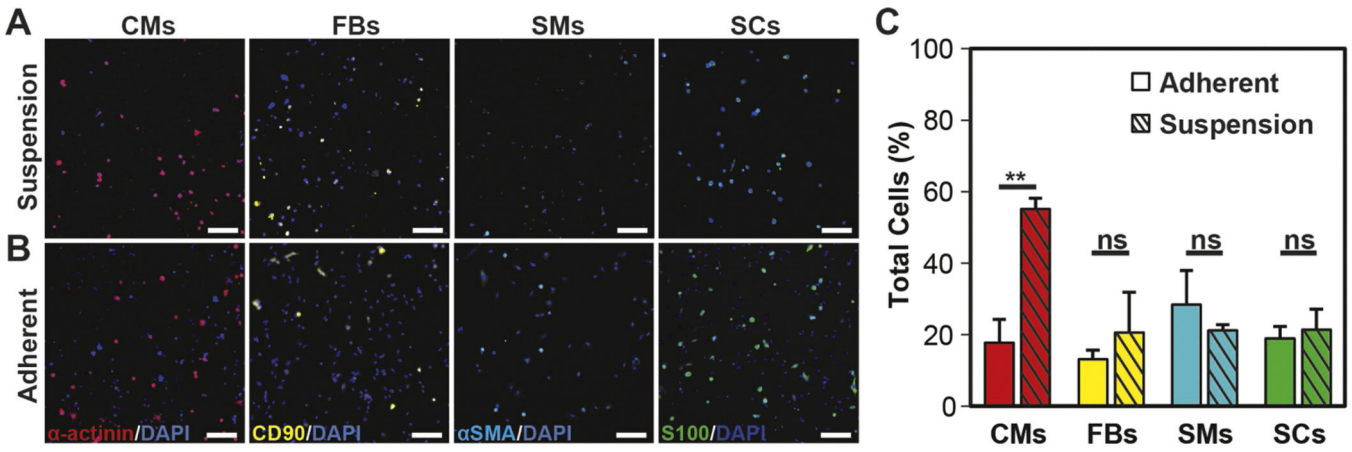

Figure 4.

Immunofluorescent quantification of cardiac cellular composition. (A) Representative suspension and (B) adherent cultures grown on fibronectin coated cover slides for 12–18 h post tissue dissociation. Cells were stained for markers for cardiomyocytes, sarcomeric alpha-actinin (red), fibroblast, CD90 (yellow), smooth muscle cells, alpha smooth muscle actin (cyan), Schwann cells, S100 (green) and cell nuclei, DAPI (blue). (C) Quantification of immunofluorescent images show that the suspension culture contains an enriched population of cardiomyocytes, with no statistical differences been other cell populations examined. (**$p < 0.05$, ns: not significant $p > 0.05$).

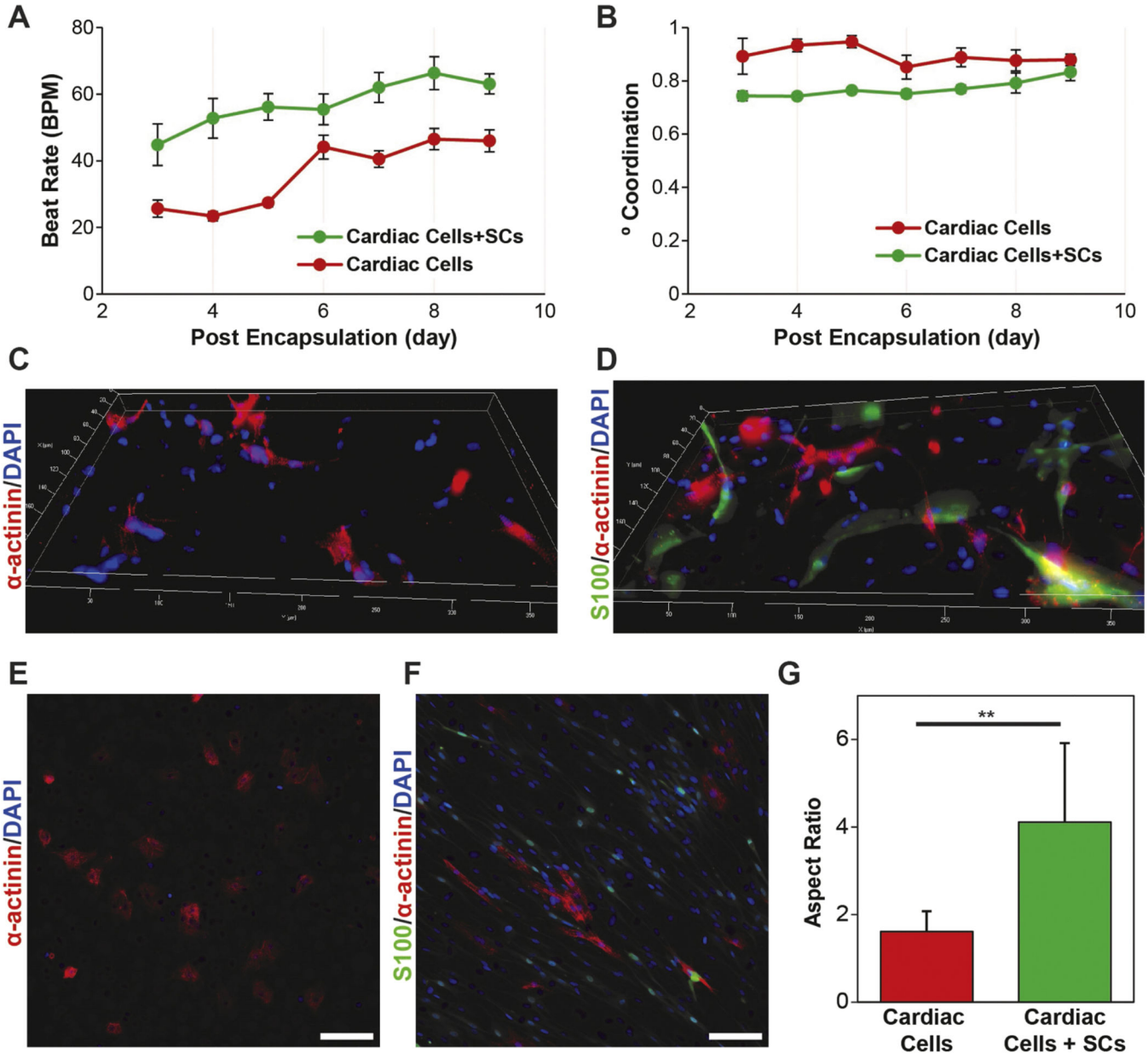

Figure 5.

Role of SCs in the 2D and 3D cardiac cell cultures. (A) Quantification ofBPMand (B) DoC for 3D μTissues over time showing that the inclusions of SCs leads to an increase and beat rate and decrease in coordinated contractions. (C) Representative immunofluorescent images of cardiac cells culture without and (D) with the inclusion of exogenous SCs encapsulated in 3D μTissues. (E) Representative immunofluorescent images of cardiac cells culture without and (F) with the inclusion of exogenous SCs in 2D (scale = 100 μm) and (G)CM aspect ratio quantification (**$p < 0.05$).

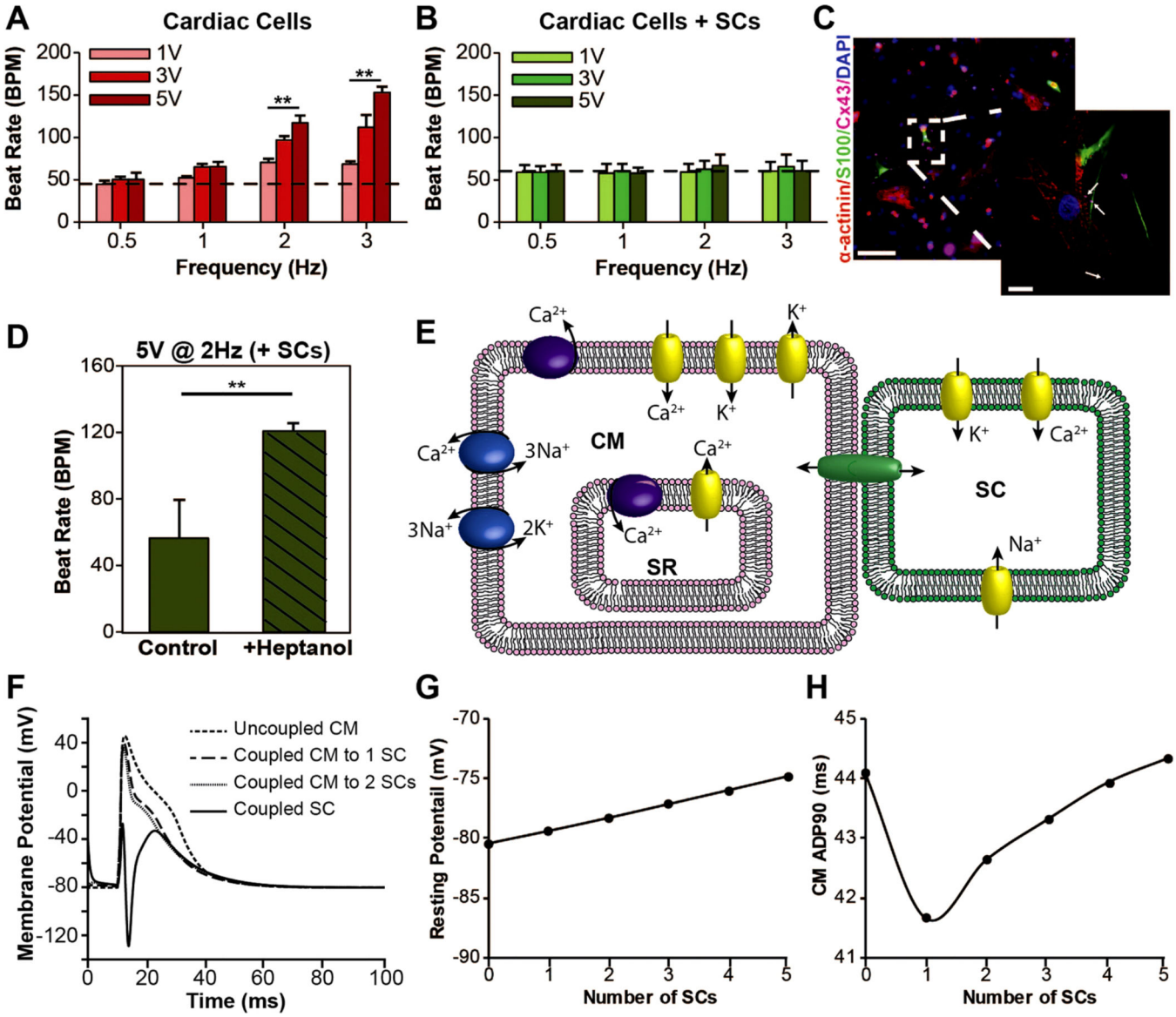

Figure 6.

External electrical pacing of 3D μTissues and computational modeling on CM-SC coupling. (A) Cardiomyocyte response to electrical stimuli at 0.5, 1, 2, and 3 Hz with increasing voltages from 1 Vto 3 Vto 5 Vshows cardiac μTissues can be paced (**$p < 0.05$), but (B) the inclusion of SCs prevents this electrical pacing (dashed line shows the average beat rate prior to electrical stimulation). (C) Representative immunofluorescent image showing the presence of connexin-43 (Cx43) junctions (purple) between CMs (red) and SCs (green) (scale = 100 μm, inlay scale = 10 μm). White arrows indicate Cx43 positive staining at the interface of SCs and CMs. (D) Electrical pacing at 2 Hz and 5 Vof individual CMs with exogenous SCs following heptanol treatment to block CMSC coupling (**$p < 0.05$). These data represent CM-beating from the same user identified cells before and after heptanol blocking ($n = 5$). (E) Schematic of a Hodgkin–Huxley model for CM-SC coupling. (F) Computational model of CM depolarization for one CM coupled to increasing numbers of

SCs overplayed with a coupled SC membrane potential. (G) Changes in CM membrane potential and (H) APD90 with increased SC coupling.